

**Spin- $\frac{1}{2}$  Heisenberg antiferromagnet on the pyrochlore lattice: An exact diagonalization study**V. Ravi Chandra<sup>1,\*</sup> and Jyotisman Sahoo<sup>2,†</sup><sup>1</sup>*School of Physical Sciences, National Institute of Science Education and Research Bhubaneswar, HBNI, Jatni, Odisha 752050, India*<sup>2</sup>*Department of Physics and Astronomy, Iowa State University, Ames, Iowa 50011, USA* (Received 11 November 2017; revised manuscript received 20 February 2018; published 12 April 2018)

We present exact diagonalization calculations for the spin-1/2 nearest-neighbor antiferromagnet on the pyrochlore lattice. We study a section of the lattice in the [111] direction and analyze the Hamiltonian of the breathing pyrochlore system with two coupling constants  $J_1$  and  $J_2$  for tetrahedra of different orientations and investigate the evolution of the system from the limit of disconnected tetrahedra ( $J_2 = 0$ ) to a correlated state at  $J_1 = J_2$ . We evaluate the low-energy spectrum, two and four spin correlations, and spin chirality correlations for a system size of up to 36 sites. The model shows a fast decay of spin correlations and we confirm the presence of several singlet excitations below the lowest magnetic excitation. We find chirality correlations near  $J_1 = J_2$  to be small at the length scales available at this system size. Evaluation of dimer-dimer correlations and analysis of the nature of the entanglement of the tetrahedral unit shows that the triplet sector of the tetrahedron contributes significantly to the ground-state entanglement at  $J_1 = J_2$ .

DOI: [10.1103/PhysRevB.97.144407](https://doi.org/10.1103/PhysRevB.97.144407)**I. INTRODUCTION**

The pyrochlore lattice is one of the earliest lattices to be investigated in the study of geometrically frustrated magnetic systems. Shortly after foundational work on the triangular lattice [1], the pyrochlore antiferromagnet was among the first three-dimensional models for which it was established that the nearest-neighbor exchange does not result in magnetic ordering and that the ground state has a finite entropy [2]—properties which are now routinely used to characterize the extent of frustration in a magnetic system. The interest in the physics of this lattice has continued unabated over several decades. Apart from intrinsic theoretical interest this is also because of the existence of real materials with this crystal structure. Examples are the spinels  $AB_2O_4$  and the  $A_2B_2O_7$  oxides [3] where the magnetic ions reside on the pyrochlore lattice. Interestingly, among the Hamiltonians that have been used to model various classes of materials with this general structure, the simple spin-1/2 nearest-neighbor Heisenberg antiferromagnet has received relatively less attention in the past. The last few years has seen a renewed interest in this system, which in part is thanks to the discovery of new materials, which can be modeled as spin-1/2 Heisenberg antiferromagnets [4–6].

Many techniques have been used to study this model and like several other magnetic systems with geometric frustration or competing interactions there is no clear consensus on the nature of the low-temperature phase. The ground-state prediction for the Hamiltonian varies with the technique used to study the problem. The ground-state manifold of a single tetrahedron of four spins, the basic unit of the lattice, consists of two degenerate singlet states. Approaches that restrict the Hilbert

space of tetrahedra to the subspace of these singlets and derive effective theories for the Hamiltonian usually result in a dimer singlet phase. This phase with broken translational symmetry has long-range order in the dimer-dimer correlations [7–12]. A power series expansion of the density matrix of the problem in powers of the intertetrahedra coupling results in a spin liquid [13] with a very short correlation length for two spin correlations. The studies based on the analysis of  $Sp(N)$  models support a (spontaneously) broken inversion symmetry [14] or the presence of several different saddle points at large  $N$  [15] but remain noncommittal about the  $SU(2)$  limit of those Hamiltonians. Fermionic mean-field theory followed by a variational Monte Carlo analysis of a mean-field state lends support to a chiral spin liquid [16,17] with long-range order in the scalar chirality operator  $\mathbf{S}_i \cdot (\mathbf{S}_j \times \mathbf{S}_k)$ , where  $(i, j, k)$  are on a tetrahedron. Finally, a finite temperature analysis using diagrammatic Monte Carlo method predicts spin ice correlations even in the Heisenberg limit [18], albeit at finite temperatures.

The focus of this paper is the analysis of the spin-1/2 nearest-neighbor antiferromagnet on the pyrochlore lattice using exact diagonalisation (ED). The principal and obvious limitation of ED studies is that we usually cannot do meaningful finite size scaling for many systems of current interest, especially if they are in two or three dimensions and the ground state is (magnetically) disordered but correlated. However, the technique does offer the advantage that for the system sizes that can be handled using this technique it provides essentially exact information about the lattices studied. We present here the results of such an ED study for the nearest-neighbor spin-1/2 antiferromagnetic pyrochlore lattice for a system size of up to 36 sites. We focus on a section of the lattice in the [111] direction and evaluate energies, and two, four, and six point correlators. In Sec. II, we introduce the Hamiltonian being studied and details of the finite size section being investigated. In Sec. III, we discuss the nature of the spectrum in the vicinity of the ground state. In Sec. IV, we present all the evaluated

\*ravi@niser.ac.in

†jsahoo@iastate.edu

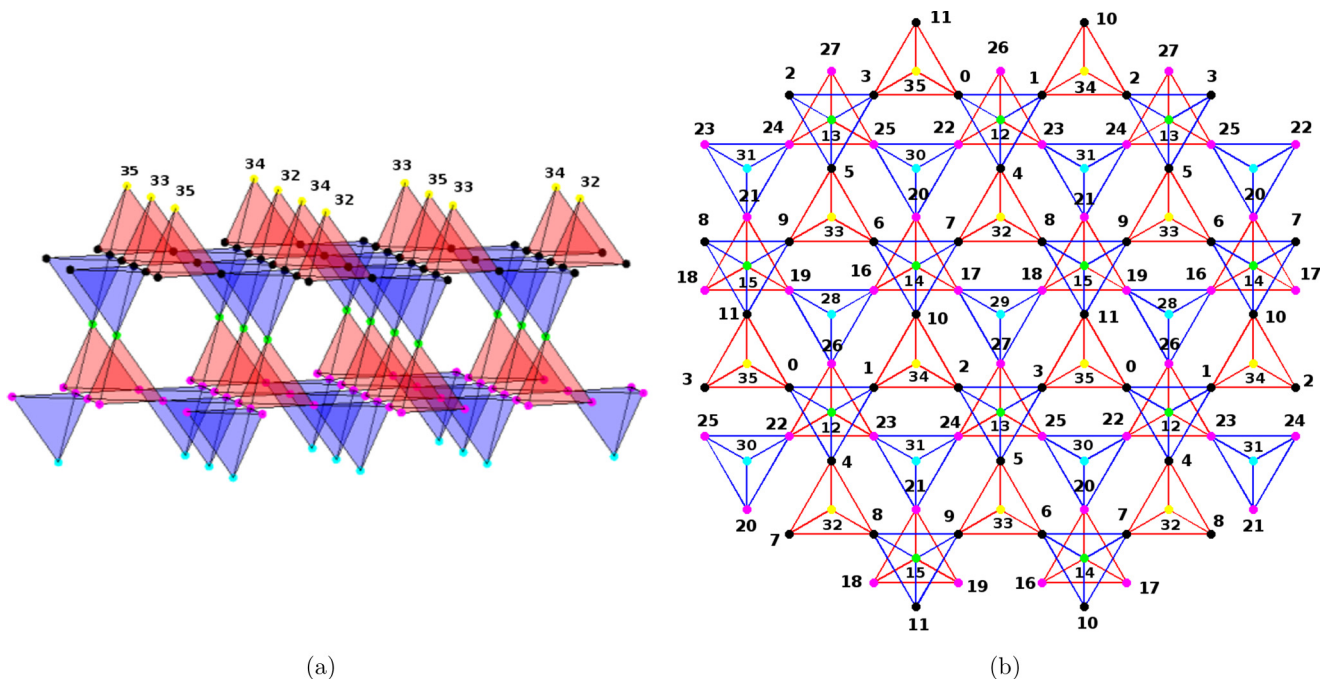


FIG. 1. The pyrochlore lattice. The figure on the right is a 2D projection with the [111] axis out of the page. The black and magenta dots are the two kagome layers and the yellow, green, and the cyan dots are the top, middle, and bottom triangular lattice layers, respectively. The numbers in the figure on the right is the site indexing used throughout the paper. The blue lines are the  $J_1$  bonds and the red lines are the  $J_2$  bonds. The top layer site labels are also presented in the 3D figure to establish the orientation.

correlations and the analysis of the ground state based on these correlations.

## II. LATTICE AND THE HAMILTONIAN

The pyrochlore lattice is a lattice of corner sharing tetrahedra, which can be seen as a face centered cubic lattice with a four-site basis (see Fig. 1). Using the conventional FCC primitive lattice vectors  $\mathbf{a}_1 = (\frac{1}{2}, \frac{1}{2}, 0)$ ,  $\mathbf{a}_2 = (0, \frac{1}{2}, \frac{1}{2})$ , and  $\mathbf{a}_3 = (\frac{1}{2}, 0, \frac{1}{2})$ , the four sublattices are  $(0, 0, 0)$ ,  $\frac{\mathbf{a}_1}{2}$ ,  $\frac{\mathbf{a}_2}{2}$ ,  $\frac{\mathbf{a}_3}{2}$ . Each site is connected to six nearest neighbors and is part of two tetrahedra of different orientation as can be seen in Fig. 1.

The model Hamiltonian being studied in this paper is

$$H = J_1 \sum_{\langle ij \rangle, A} \mathbf{S}_i \cdot \mathbf{S}_j + J_2 \sum_{\langle ij \rangle, B} \mathbf{S}_i \cdot \mathbf{S}_j, \quad (1)$$

where  $\mathbf{S}_i$  are spin-1/2 operators at the sites of the pyrochlore lattice.  $J_i$  are nearest-neighbor antiferromagnetic coupling constants for the tetrahedra of two different orientations ( $J_1$  for blue and  $J_2$  for red tetrahedra in Fig. 1). The parameter in the problem is  $J_2$  ( $J_1$  is set to 1 and so is  $\hbar$ ). This Hamiltonian is called the breathing pyrochlore Hamiltonian [4].

We study a finite part of the lattice shown in Fig. 1(a) using exact diagonalization. Figure 1(b) shows a 2D projection of the system studied with site labels. The data for two system sizes of 28 and 36 sites have been analyzed in detail in this paper. The lattice of 28 sites is obtained by omitting sites in the bottom and top triangular layers. Periodic boundary conditions are imposed in the kagome and triangular lattice planes. The site indexing used to label the different sites shown in Fig. 1(b) will be used in the rest of the paper.

We employ the conservation of the  $S_z^{\text{total}} = \sum_i S_{iz}$  and the spin inversion symmetry in the  $S_z^{\text{total}} = 0$  sector to reduce the size of the Hilbert space. Using these two symmetries, the Hilbert space dimension of the 36-site system is 4 537 567 650. The Lanczos algorithm [19] is used throughout for computations of the ground state and low-lying excitations.  $J_2$  is varied from 0.0 to 2 and is the parameter in the problem and corresponds to the  $x$  axis (which starts at  $J_2 = 0.05$ ) in all plots unless mentioned otherwise. We note that the  $J_2 > 1$  region is of course physically the same as a section of the  $J_2 < 1$  region since for finite-size systems considered here it simply corresponds to exchanging the roles of the two kinds of tetrahedra. Nevertheless, we present data for the whole range mentioned as an additional explicit consistency check. There are several  $J_2$  values for which using the above mentioned two symmetries still result in doubly degenerate lowest eigenvalues in the symmetry sector containing the ground state. This degeneracy stems from the symmetry of the Hamiltonian under certain permutations of site indices, which are elements of the automorphism group for this graph. We choose one such permutation to extract orthogonal states with distinct symmetry labels for  $J_2$  values where degeneracy of the ground state is present. The used permutation of site labels for the results presented in this paper is detailed in Appendix, and in the rest of the text is denoted by  $\mathcal{P}$ . The same symbol is used to denote the operator for that permutation of site indices or the eigenvalues of that operator where necessary. We have verified that the computed energy eigenvalue and the energy expectation value that can be derived using the computed correlations match to at least  $10^{-6}$ . All explicitly stated numbers have been quoted with 6 significant digits, though several numbers are much more accurate.

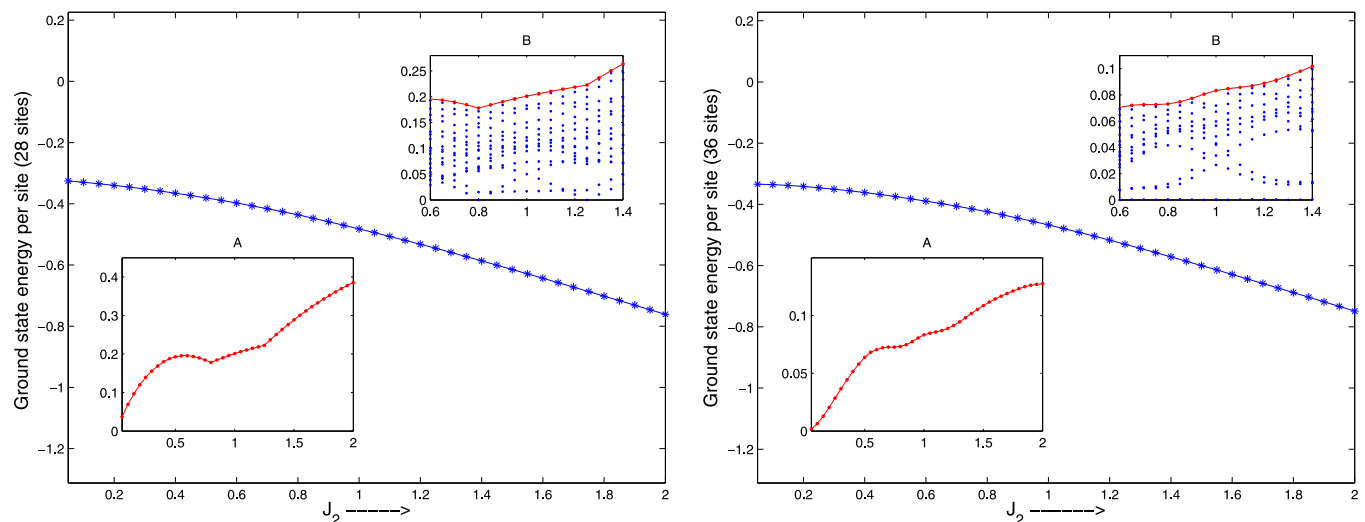


FIG. 2. The ground-state energy per site and the nature of the low-energy spectrum as a function of  $J_2$ . The left figure is for the 28-site cluster and the right figure for the 36-site cluster. The inset labeled A shows the spin gap (the energy difference between the lowest magnetic excitation and the singlet ground state) and the inset labeled B shows the presence of singlet excitations below the spin gap (blue markers) near  $J_2 = 1$ . Energy eigenvalues plotted are for the Hamiltonian in Eq. (1) with  $J_1$  and  $\hbar$  set to 1. See Sec. III for details.

At this point, it is pertinent to recall some elementary properties of the basic tetrahedral unit, which play a role in the analysis of the evaluated correlation functions. A single tetrahedron with all equal strength antiferromagnetic bonds has as its ground state two degenerate singlets. This follows directly from the fact that the Hamiltonian of the tetrahedron itself is simply equal to  $H_{\text{tetrahedron}} = \frac{J}{2}(\sum_i \mathbf{S}_i)^2 - \frac{3J}{2}$ . There are distinct ways of thinking about this space of degenerate ground states, which leads to consideration of different kinds of ordered states on the full lattice. One obvious way is to group the four spins into distinct pairs of spins (say [12][34]). Then we can build total spin singlets by either considering a direct product of singlets of each pair or by constructing a spin-0 state using the triplet states of each pair. The dimer-dimer correlation  $\langle(\mathbf{S}_1 \cdot \mathbf{S}_2)(\mathbf{S}_3 \cdot \mathbf{S}_4)\rangle$  for the former is  $9/16$  and  $1/16$  for the latter. However, one could equally consider the Hamiltonian of the tetrahedron to be a sum of Hamiltonians defined on the triangular faces of the tetrahedron:  $H = \frac{1}{2} \sum_{\Delta} H_{\Delta} = \frac{1}{2} \sum_{ijk} (\mathbf{S}_i \cdot \mathbf{S}_j + \mathbf{S}_j \cdot \mathbf{S}_k + \mathbf{S}_k \cdot \mathbf{S}_i)$ , where the sum is over all distinct triads of spins ( $ijk$ ) on the tetrahedron. It is well known [20] that  $\Xi_{ijk} = \mathbf{S}_i \cdot (\mathbf{S}_j \times \mathbf{S}_k)$  commutes with  $\sum_i \mathbf{S}_i$  and hence the eigenstates of  $H_{\text{tetrahedron}}$  can be expressed as eigenstates of  $\Xi_{ijk}$  belonging to a face of a tetrahedron. Furthermore, if we focus on only the two-dimensional ground-state singlet manifold then suitable linear combinations, which are simultaneous eigenstates of all  $\Xi_{ijk}$  can be constructed [20]. Also,  $(\Xi_{ijk})^2 = \frac{3}{32} - \frac{1}{8}H_{\Delta}$ , for spin  $1/2$ . Thus the full Hamiltonian on the lattice can be written either as a sum of total spin operators on tetrahedra or the sum of the squares of  $\Xi_{ijk}$  operators on all triangles of the lattice. Given this structure of the ground-state manifold of the basic tetrahedral unit and the Hamiltonian, Eq. (1) appears to be a natural candidate (especially at  $J_1 = J_2$ ) to explore spontaneous dimerization [7–12] or long-range chiral order in three dimensions [16,17]. We will analyze those possibilities from the point of view of exact diagonalization calculations in the following sections.

### III. LOW-ENERGY SPECTRUM

We begin with a description of the low-energy spectrum of the system for the two lattice sizes considered. Figure 2 shows the variation of the ground-state energy per spin as a function of  $J_2$ . The values of the energies for two sizes at the point  $J_2 = J_1 = 1$  are  $-0.482081$  (28 sites) and  $-0.466971$  (36 sites), respectively. The difference in the energy per site values of these two lattice sizes for other  $J_2$  values is of similar magnitude or smaller.

The insets in the figures show some details of the excitation spectrum above the ground state. Inset A shows the variation of the spin gap with  $J_2$ . Inset B depicts the low-energy excitations below the lowest nonsinglet state in a region close to  $J_2 = 1$ . The ground state and the lowest nonmagnetic excitation, which is the lowest energy state in a different symmetry sector, are fully converged, in the Lanczos sense. The singlets within that gap are partially converged to various degrees of accuracy at that Lanczos iteration. However, the changes of their energies with iterations indicate that almost all of them are expected to be in the gap region after convergence to high accuracy. The spin gap for the 28 and 36 site systems are  $0.201229$  and  $0.083273$ , respectively, for  $J_2 = 1$ .

As can be seen for both the lattice sizes there are several singlet excitations below the lowest energy magnetic state. This is a feature that has been seen in ED studies of other frustrated magnetic systems [21–23], most well known among them being the kagome antiferromagnet. We would like to note that the density of singlets below the magnetic gap depends on the boundary conditions imposed. For example, whereas about 180 states below the lowest magnetic states are known for the 36 site system of the kagome lattice with periodic boundary conditions [21], the number drops down to only a few for the same system with open boundary conditions. In our system, we have periodic boundary conditions in two directions. The singlet gap for the 28-site system is  $0.016832$  whereas for the 36-site system it is  $0.000143$  for  $J_2 = 1$ . It is not immediately

TABLE I. Spectrum and correlations in the ground state for  $J_2 = 1$ .  $\phi_{i-j}$  denotes  $\mathbf{S}_i \cdot \mathbf{S}_j$  and  $\Xi_{i-j-k}$  denotes  $\mathbf{S}_i \cdot (\mathbf{S}_j \times \mathbf{S}_k)$ .  $\langle \rangle$  denotes the expectation value in the ground state. The site indices follow the indexing shown in Fig. 1(b). Missing numbers in the second column correspond to correlations that contain sites not present in the 28-site system.

Property	28 sites	36 sites
Ground-state energy per spin	-0.482081	-0.466971
Spin gap	0.201229	0.083273
$\langle (\mathbf{S}_o \cdot \mathbf{S}_i) \rangle_{1\text{-bond}}$	-0.192600	-0.168562
$\langle (\mathbf{S}_o \cdot \mathbf{S}_i) \rangle_{2\text{-bond}}$	0.035057	0.028212
$\langle (\mathbf{S}_o \cdot \mathbf{S}_i) \rangle_{3\text{-bond}}$	-0.014860	-0.008655
$\langle \phi_{0-12}\phi_{1-4} \rangle, \langle \phi_{0-1}\phi_{4-12} \rangle, \langle \phi_{0-4}\phi_{1-12} \rangle$	0.152902	0.093991
$\langle \phi_{0-12}\phi_{6-14} \rangle$	0.074815	0.046312
$\langle \phi_{0-12}\phi_{2-13} \rangle$	0.016658	0.016217
$\langle \phi_{0-12}\phi_{23-31} \rangle$		0.040566
$\langle \phi_{12-26}\phi_{22-23} \rangle, \langle \phi_{12-23}\phi_{22-26} \rangle, \langle \phi_{12-22}\phi_{23-26} \rangle$	0.152902	0.093991
$\langle \phi_{12-26}\phi_{13-27} \rangle$	0.074815	0.046312
$\langle \phi_{12-26}\phi_{14-20} \rangle$	0.016657	0.016217
$\langle \phi_{12-26}\phi_{10-34} \rangle$		0.038405
$\langle \Xi_{1-4-12}\Xi_{1-4-12} \rangle$	0.159053	0.151897
$\langle \Xi_{12-23-26}\Xi_{12-23-26} \rangle$	0.159053	0.151897
$\langle \Xi_{4-8-32}\Xi_{4-8-32} \rangle$		0.171852
$\langle \Xi_{21-24-31}\Xi_{21-24-31} \rangle$		0.171852
$\langle \Xi_{1-4-12}\Xi_{7-10-14} \rangle$	0.020505	0.030824
$\langle \Xi_{1-4-12}\Xi_{3-5-13} \rangle$	0.016554	0.006981
$\langle \Xi_{1-4-12}\Xi_{21-24-31} \rangle$		-0.000230
$\langle \Xi_{1-4-12}\Xi_{18-27-29} \rangle$		0.000141

clear if the rather small size of the singlet gap for the 36-site system is an artefact of our specific finite size geometry. We have, however, explicitly verified that it is indeed a genuine excitation with the computed energy and not an artefact of the loss of orthogonality affecting the Lanczos vectors [19]. We cannot predict the fate of this small gap at larger length scales. We now present various spin correlations in the system to obtain a more detailed characterization of the ground state.

#### IV. GROUND-STATE CORRELATIONS

We evaluated the spin-spin ( $\langle \mathbf{S}_i \cdot \mathbf{S}_j \rangle$ ), dimer-dimer ( $\langle \phi_{ij} \cdot \phi_{kl} \rangle$ ,  $\phi_{ij} \equiv \mathbf{S}_i \cdot \mathbf{S}_j$ ), and scalar spin chirality correlations ( $\langle \Xi_{ijk} \cdot \Xi_{lmn} \rangle$ ,  $\Xi_{ijk} \equiv \mathbf{S}_i \cdot (\mathbf{S}_j \times \mathbf{S}_k)$ ) for the ground state of the Hamiltonian as a function of  $J_2$ . We discuss below in turn these three correlations to analyse the zero-temperature phase of the system. Table I shows detailed information about the spectrum and spin correlations for  $J_2 = 1$  and we will refer to it frequently in the following. As described in Introduction, this is the point in the phase diagram which has received most attention and has been conjectured to harbor several different kinds of ground states. The ground state for this point is a nondegenerate singlet, which belongs to the eigenvalue  $-1$  for the site permutation operator  $\mathcal{P}$ . We note that the 28-site system has several incomplete tetrahedra whereas all sites of the 36-site system are part of (at least one) tetrahedron which has all six bonds. To that extent, the correlations of latter system are expected to have properties more aligned with the full lattice. For this reason, unless mentioned otherwise, the plots in this section are all for the system with 36 sites.

#### A. Two spin correlations

We begin with a brief description the behavior of the two spin correlations  $\langle \mathbf{S}_o \cdot \mathbf{S}_i \rangle$ . We evaluate these correlations using the site with index 0 as the reference site [see Fig. 1(b)]. For  $J_2 = 1$  in Table I,  $\langle (\mathbf{S}_o \cdot \mathbf{S}_i) \rangle_{1\text{-bond}}$  means the average of correlations with all sites which can be reached from site 0 by crossing one bond. Analogous meanings follow for the other two correlations. As can be seen very clearly, the correlations decay rapidly with distance. This rapid decay is consistent with an expectation of a magnetically disordered ground state in this highly frustrated system and has been reported in earlier analyses [13]. Choosing another site as a reference site might result for this finite size system in (quantitatively) different behavior since translational invariance is absent in the third direction. However, we have verified that the general trend of rapid decay holds and does so for all values of  $J_2$ . We will not present here further details of two-point correlations as the general feature that correlations weaken significantly beyond the smallest length scale is true for all  $J_2$ . We present in the following sections higher-order spin correlations.

#### B. Dimer-dimer correlations

We now study the dimer-dimer correlations in the ground state. They are denoted in the paper by  $\langle \phi_{i-j}\phi_{k-l} \rangle$  where  $\phi_{i-j} \equiv \mathbf{S}_i \cdot \mathbf{S}_j$ .

In the Table I we show some relevant dimer-dimer correlations for  $J_2 = 1$ . The table shows two different kinds of dimer-dimer correlations. The first are ( $\langle \phi_{0-12}\phi_{1-4} \rangle$ ,  $\langle \phi_{0-1}\phi_{4-12} \rangle$ ,  $\langle \phi_{0-4}\phi_{1-12} \rangle$ ) and ( $\langle \phi_{12-26}\phi_{22-23} \rangle$ ,  $\langle \phi_{12-23}\phi_{22-26} \rangle$ ),

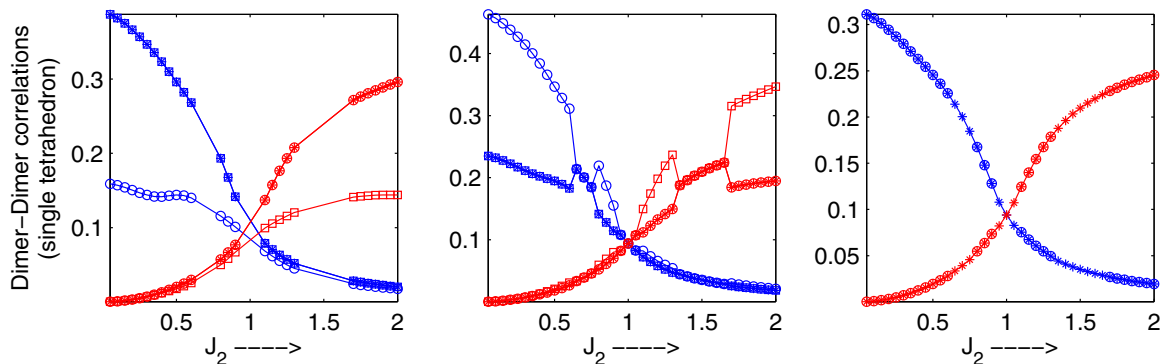


FIG. 3. The variation with  $J_2$  of dimer-dimer correlations within a single tetrahedron for the 36 site cluster. Left figure and middle figures are for eigenvalue  $+1$  and  $-1$ , respectively, of the site permutation operator  $\mathcal{P}$  detailed in Appendix. The markers indicate the following correlations in the ground state ( $\phi_{ij} \equiv \mathbf{S}_i \cdot \mathbf{S}_j$ ): blue stars  $\rightarrow \langle \phi_{0-1}\phi_{4-12} \rangle$ , blue circles  $\rightarrow \langle \phi_{0-4}\phi_{1-12} \rangle$ , blue squares  $\rightarrow \langle \phi_{1-4}\phi_{0-12} \rangle$ , red stars  $\rightarrow \langle \phi_{12-26}\phi_{22-23} \rangle$ , red circles  $\rightarrow \langle \phi_{12-23}\phi_{22-26} \rangle$ , and red squares  $\rightarrow \langle \phi_{12-22}\phi_{23-26} \rangle$ . The figure on the right shows the average of all the three correlations within a tetrahedron. The blue markers are for the  $J_1$  tetrahedron red for the  $J_2$  tetrahedron as in the other two figures. The open circles are for eigenvalue  $+1$  and the stars are for eigenvalue  $-1$  of  $\mathcal{P}$ .

( $\phi_{12-22}\phi_{23-26}$ )), which are the three possible dimer-dimer correlations within a tetrahedron, the former being a  $J_1$  tetrahedron and the latter a  $J_2$  tetrahedron. At  $J_2 = 1$ , all the three different dimer-dimer correlations have the same value.

Figure 3 shows the same dimer-dimer correlations as a function of  $J_2$ . The three pairs of nearest-neighbor correlations in a tetrahedron have been shown explicitly. It is clear from this figure that the system passes through several regions where the ground state is doubly degenerate, as mentioned earlier. These distinct regions in the plot are tabulated in Table II and the degeneracy is indicated using the eigenvalue of the site permutation operator  $\mathcal{P}$ . It can be seen that whenever the ground state is nondegenerate the three different dimer-dimer spin correlations within a tetrahedron are all equal. In case of degeneracy, the symmetry between the dimers is broken and results in the different values for particular dimer-dimer correlations in the two eigenstates. We note that how exactly the broken symmetry manifests itself depends on the chosen permutation of site indices. For our chosen permutation,  $\langle \phi_{0-1}\phi_{4-12} \rangle$  and  $\langle \phi_{1-4}\phi_{0-12} \rangle$  have the same value in case of degeneracy and  $\langle \phi_{0-4}\phi_{1-12} \rangle$  has a different value. This might change if we had chosen another permutation from

TABLE II. The different regions of  $J_2$  and eigenvalue of the symmetry operator  $\mathcal{P}$  for the ground state of the 36-site cluster. Entries with only one eigenvalue for  $\mathcal{P}$  correspond to a nondegenerate ground state. (Note: we vary  $J_2$  in increments of 0.05.)

$J_2$ range	Eigenvalue of $\mathcal{P}$
(0,0.6)	(+1, -1)
(0.65,0.75)	(-1)
(0.8,0.9)	(+1, -1)
(0.95,1.05)	(-1)
(1.1,1.3)	(+1, -1)
(1.35,1.65)	(-1)
(>1.65)	(+1, -1)

the automorphism group to extract distinct symmetry labels for the eigenstates.

The figure on the right in Fig. 3 shows the average of the three dimer correlations at any  $J_2$ . The effect of the degeneracy is not visible in this plot and we get a single crossing at  $J_2 = 1$ . The general trend of the plots is similar for the 28-site system, though there the regions where the eigenvalue is degenerate are different. Thus the details of the existence and locations of the several crossings might be dependent on the nature of the finite size system and the boundary conditions. However, if we consider the full tetrahedron (by considering an average as above) then at least from the point of view of dimer-dimer correlations within a single tetrahedron there is a smooth evolution from the state of disconnected tetrahedra at  $J_2 = 0$  to the state in the vicinity of  $J_2 = 1$ .

We would like to understand in a bit more detail how the tetrahedral unit evolves within the system from  $J_2 = 0$  to  $J_2 = 1$ . To that end, we analyze quantitatively how the tetrahedron is entangled with the rest of the lattice. In order to do that, we make use of the property of Schmidt decomposition of a pure state. We know that a pure state of any quantum system (say  $|\psi\rangle$ ) partitioned into two parts (say  $A$  and  $B$ ) can be written as

$$|\psi\rangle = \sum_{\lambda} \sqrt{\lambda} |\lambda\rangle_A \otimes |\lambda\rangle_B. \quad (2)$$

Here,  $\lambda$  are real and positive and the number of the terms in the sum is at most the smaller of the Hilbert space dimensions of  $A$  and  $B$ .  $|\lambda\rangle_{A/B}$  are Schmidt vectors for the partition for a given  $\lambda$  and  ${}_A\langle\lambda|\lambda'\rangle_A = {}_B\langle\lambda|\lambda'\rangle_B = \delta_{\lambda,\lambda'}$ . The Schmidt vectors can also be shown to be the eigenvectors of the reduced density matrix of the partition with the eigenvalue  $\lambda$ .

Usual studies of entanglement content of lattice models [24] involve partitioning the system of interest into two blocks to study the scaling of entanglement entropy as the size of one of the partitions is increased. However, Schmidt decomposition can also be used to directly probe the part of the Hilbert space of a partition responsible for entangling it with the whole system. Here we choose the basic tetrahedral unit as one of our

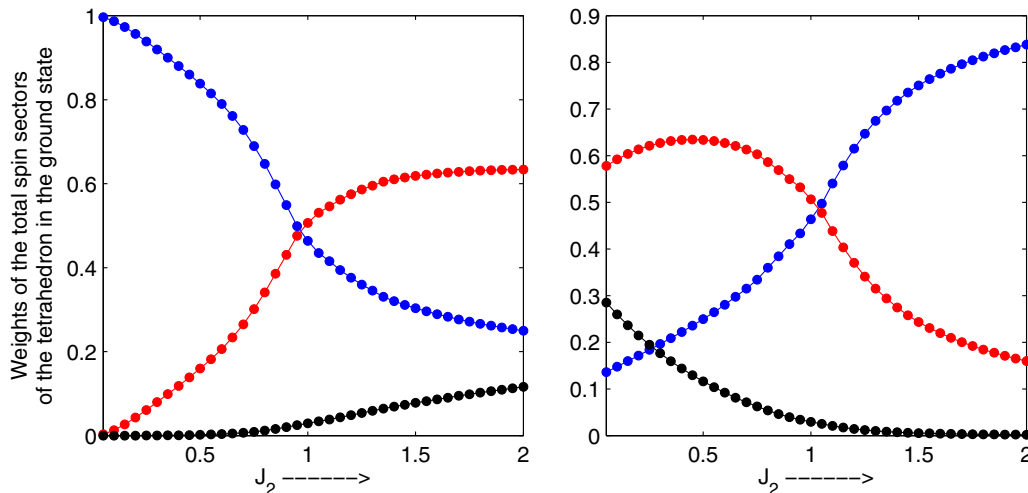


FIG. 4. The weights of the different total spin sectors of the tetrahedron in the Schmidt decomposed ground state [see Eq. 2 and the following discussion] with a tetrahedron as one of the partitions. We have shown data for the 36-site system and the  $\mathcal{P} = -1$  symmetry sector. The blue, red, and black markers denote the weights of the singlet, triplet, and quintet sectors of the tetrahedron. The figure on the left is for a  $J_1$  tetrahedron [sites (0, 1, 4, 12)] and the one on the right is for a  $J_2$  tetrahedron [sites (12, 22, 23, 26)]. Weights add to 1 as is to be expected for reduced density matrix eigenvalues.

partitions. Our objective is to check quantitatively which states of the tetrahedral Hilbert space are principally responsible for its entanglement with the rest of the lattice and with what weight. Since the ground state is a singlet and the system is bipartitioned, the Schmidt vectors can be labeled using a total spin label for the tetrahedron and the sum of  $\lambda$  values corresponding to a particular total spin directly gives the weight of that total spin sector in the Schmidt decomposition.

Figure 4 shows the spin weights corresponding to the three total spin sectors  $S_{\text{total}} = 0, 1, 2$  in the tetrahedron in the Schmidt decomposition. We have only shown results for the ground state in the  $\mathcal{P} = -1$  sector, the sector  $\mathcal{P} = 1$  is similar except for missing data points in regions where the ground state is nondegenerate with  $\mathcal{P} = -1$  (see Table II). We see that as the system evolves from  $J_2 = 0$  where the tetrahedra are disconnected from each other, the weight of the triplet sector of the tetrahedral Hilbert space grows progressively at the expense of the singlet sector which is the only relevant sector at  $J_2 = 0$ . Notably, the weight contributed by the triplet sector of the tetrahedron near  $J_2 = 1$  is not a subdominant fraction of the total weight but is almost equal to the weight contributed by the singlet sector. Hence effective theory formulations which rely on discarding the nonsinglet states of a tetrahedron in effect discard a part of the Hilbert space, which is as important as the singlet sector from the point of view of entanglement of the tetrahedron with the rest of the lattice.

In addition to the weights of the total spin sectors, which depend on  $\lambda$ , one can also study the structure of individual Schmidt vectors to gain detailed information about the way different possible states in a sector contribute to the total weight of that sector. For instance, one can explicitly evaluate the weights contributed by the two possible total spin singlets on the tetrahedron to the overall weight contributed by the singlet sector shown in Fig. 4. Such a computation shows that the two degenerate eigenvectors (when present) differ by the weights contributed by the two singlets simply being exchanged with

each other. In case of nondegenerate ground states, the two kinds of singlets contribute equal weight. This essentially is the microscopic reason for the structure of the dimer-dimer correlations plots shown in Fig. 3.

The analysis of the ground state just presented, involving Schmidt decomposition with a basic unit of the lattice as a partition, is of course general and it can be used to gain information about the ground state structure of other spin Hamiltonians. As the size of the cluster of interest increases, this approach enables us to extract information that may not be easily accessible using correlation functions.

Another set of dimer-dimer correlations shown in Table I are correlations between dimers on different tetrahedra. Figure 5 shows these correlations as a function of  $J_2$  for the 36 site cluster. The plot on the left is for the ground state with eigenvalue  $+1$  of the permutation operator  $\mathcal{P}$  and figure on the right are for eigenvalue  $-1$ . These correlations have been analyzed to probe the possibility of order in dimer-dimer correlations, which has been discussed [7–10] as one of the possible low-temperature states at  $J_2 = 1$ . As can be seen by comparing Figs. 3 and 5 (dimer-dimer correlations within and between tetrahedra), there is an extended region till about  $J_2 \sim 0.75$  where these correlations between tetrahedra remain strong and sometimes comparable to the correlations within a single tetrahedron, something we would expect in a state with dimer order. Following this, we see a drop in correlations to low values, which are smaller than the correlations within a tetrahedron. This is also the time when the disparity between the dimer correlations belonging to tetrahedra of different orientation (blue and red markers in the plot) start reducing sharply. This is something we would expect on general grounds as the system approaches  $J_2 = 1$ . In this region, while there is a decrease of the correlation with distance as can be seen in Table I and Fig. 5, it is clearly not as rapid as in the case of the two-point correlator. As a result, while it is clear that the system goes to a qualitatively different phase, the currently

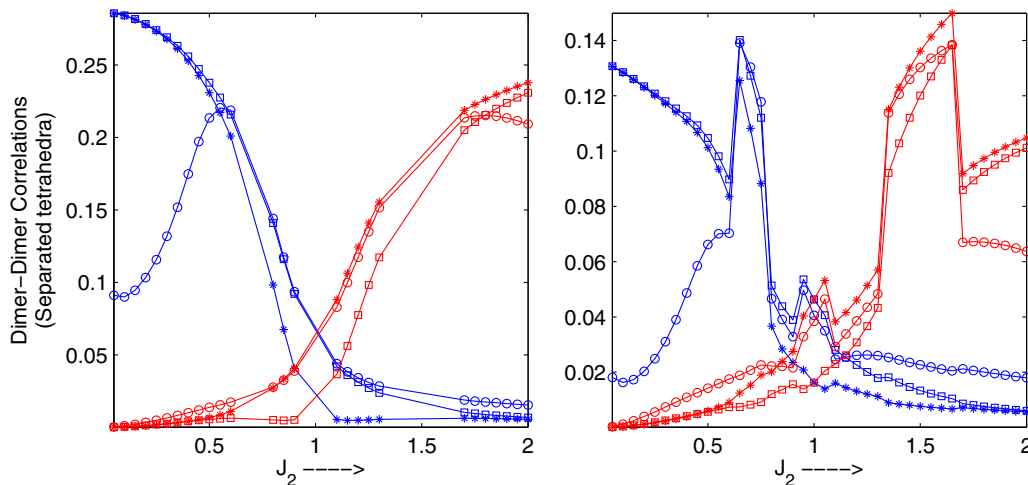


FIG. 5. Dimer-dimer correlations ( $\langle \phi_{ij} \phi_{kl} \rangle$ ,  $\phi_{ij} \equiv \mathbf{S}_i \cdot \mathbf{S}_j$ ) in the ground state across different tetrahedra as a function of  $J_2$ . ( $ij$ ) is the (0 – 12) for blue symbols and (12 – 26) for the red symbols. ( $kl$ ) are (6 – 14) (blue squares), (2 – 13) (blue stars), (23 – 31) (blue circles), (13 – 27) (red stars), (10 – 34) (red circles), (14 – 20) (red squares). The plot on the left is for eigenstate with  $\mathcal{P} = 1$  and the right for  $\mathcal{P} = -1$ . All data shown in this plot is for the 36-site cluster.

available data are not sufficient to conclusively rule out some remnant weak dimer order near  $J_2 = 1$ .

### C. Chirality correlations

In Sec. II, we noted that the low-energy degenerate ground-state manifold of the elementary tetrahedral unit makes this system a promising candidate for exploring long-range chiral order. We now present the evaluation of chirality correlations in this system. They are denoted by  $\langle \Xi_{i-j-k} \Xi_{l-m-n} \rangle$ , where  $\Xi_{i-j-k} \equiv \mathbf{S}_i \cdot (\mathbf{S}_j \times \mathbf{S}_k)$  and as usual we evaluate the expectation value in the ground state. The evaluated chirality correlations are shown in Table I for  $J_2 = 1$ . The same correlations are shown as a function of  $J_2$  in Fig. 6 for 36 sites. The plots on the right are for correlations of the form ( $\langle \Xi_{i-j-k} \Xi_{l-m-n} \rangle$ ) and the two triangles involved belong to different tetrahedra. It is clear from these plots that these correlations do decay very quickly as can be seen both in the plots and for  $J_2 = 1$  in Table I. While it is not feasible at these lattice sizes to directly compare predicted values for the chiral order parameter [16,17], any presumed decay at this rate for a few more lattice spacings would result in the order parameter being very small.

Variational Monte Carlo evaluations, which predict chiral order, usually involve imposing uniformity in the nearest-neighbor two-spin correlations when choosing an ansatz for the mean-field analysis. Our calculations have open boundary conditions in the third direction and that essentially means all two spin correlations are not equivalent. We would like to check how severe is the effect of open boundary conditions. The plots on the left in Fig. 6 are for correlations of the form ( $\langle \Xi_{i-j-k} \Xi_{i-j-k} \rangle$ ) and these have been evaluated to get an indication of the effect of open boundary conditions in the [111] direction. The open symbols correspond to a  $\Xi_{i-j-k}$  with the triangle being part of a tetrahedron which contains a site from the triangular lattice layer at the bottom or top in Fig. 1. The full symbols correspond to a tetrahedron in the interior in which each site is participating in six bonds. We note that the

open symbols are consistently above the full symbols for all  $J_2$ . From the plot it is clear that the triangle on the boundary is more likely to behave akin to an “isolated” tetrahedron. We note that for a single tetrahedron ( $\langle \Xi_{i-j-k} \Xi_{i-j-k} \rangle$ ) has a value of 0.1875 in the ground state. This can be compared with 0.151897 for the triad (1 – 4 – 12) and 0.171852 for the triad (4 – 8 – 32) in our case for  $J_2 = 1$ . Furthermore, we have checked that for a 32-site cluster with periodic boundary conditions the value of this correlator is 0.158357 for  $J_2 = 1$ . These results empirically indicate that the effect of open boundary conditions in the third direction in our problem is probably not so severe as to render a possible chiral ordered state undetectable. Nevertheless, a computation using a larger lattice size can help putting this claim on a stronger footing.

## V. SUMMARY AND DISCUSSION

This study hopes to contribute to the existing understanding of the spin-1/2 antiferromagnet on the pyrochlore lattice from an exact diagonalization perspective. From the point of view of the nature of the low-lying spectrum and the two spin correlations, the system shares common features of quantum frustrated magnetism also found in other systems. The short length scale of spin correlations is one such feature for  $J_2 = 1$  and our study confirms that, though at this lattice size we cannot formally extract a correlation length. We have also shown the presence of several low-lying singlet excitations below the magnetic gap.

We investigated the dimer-dimer and scalar chirality correlations in some detail in Sec. IV. Briefly, we can say that while not being entirely conclusive, the ED data for the system we have studied do not strengthen the case for the existence of these orders at  $J_2 = 1$ .

In case of the dimer-dimer correlations, several of the earlier predictions involve a starting point where the Hilbert space of the tetrahedral unit is truncated to the two degenerate singlets. We showed using an analysis of the Schmidt coefficients that result from using the tetrahedron as one of the partitions that

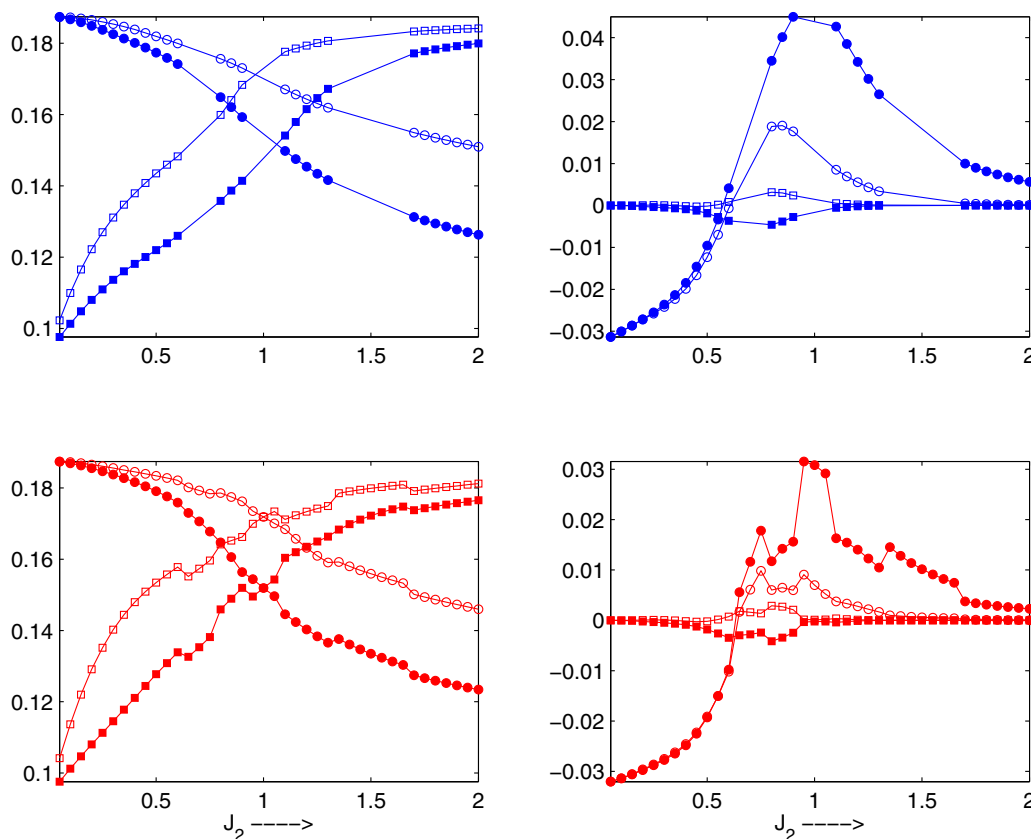


FIG. 6. The variation of chirality correlations ( $\langle \Xi_{i-j-k} \Xi_{i-m-n} \rangle$ ,  $\Xi_{i-j-k} \equiv \mathbf{S}_i \cdot (\mathbf{S}_j \times \mathbf{S}_k)$ ) with  $J_2$  for the ground state of the 36-site cluster. The two plots on the top are for  $\mathcal{P} = 1$  (blue markers) and the two plots on the bottom for  $\mathcal{P} = -1$  (red markers). The plots on the left are for correlations  $\langle \Xi_{i-j-k} \Xi_{i-j-k} \rangle$  [( $ijk$ ) same in both triangles]. ( $i-j-k$ ) are given by (1-4-12) (filled circles), (12-23-26) (filled squares), (4-8-32) (empty squares), and (21-24-31) (empty circles). The two figures on the right are chirality correlations for separated triangles:  $\langle \Xi_{1-4-12} \Xi_{7-10-14} \rangle$  (filled circles),  $\langle \Xi_{1-4-12} \Xi_{3-5-13} \rangle$  (empty circles),  $\langle \Xi_{1-4-12} \Xi_{21-24-31} \rangle$  (filled squares), and  $\langle \Xi_{1-4-12} \Xi_{18-27-29} \rangle$  (empty squares). Note that the number of bonds to be crossed to go from one triangle to the other is larger for the open symbols compared to the closed ones.

the triplet sector of the tetrahedron contributes almost an equal weight near  $J_2 = 1$ . This fact in conjunction with the observation that dimer correlations are small and decaying (albeit slowly) leads us to suspect that dimer order even if it is present is likely to be very weak. For the chirality correlations, we find that the decay is more rapid than in the case of dimer-dimer correlations and the value of correlations is quite small. We note here, as also pointed out in the discussion regarding Fig. 3 in Sec. IV B, that the seemingly abrupt changes in correlations in Figs. 3, 5, and 6 have their origins in the degeneracy of the spectrum for this specific cluster. We have verified that for a smaller cluster of 32 sites with fully periodic boundary conditions (where the data does not have such abrupt changes), all the statements about the lack of the studied orders still hold.

In order to make the claims of the lack of the above orders stronger it is important to evaluate the same correlations for a larger symmetric cluster which can give access to more separation between the dimers and triangles involved in the evaluated correlations. One clear way of doing this would be to add another kagome layer of 12 sites in Fig. 1(a) and then coupling it to the triangular lattice layer on the other side using periodic boundary conditions. This would result in a fully periodic cluster of 48 spins. This lattice size, though accessible

with current technology [25], is considerably more involved and is beyond the scope of this paper. We can not also in this work comment on dynamical correlations of this model, which might have a bearing on the detailed description of the nature of the possible  $T \rightarrow 0$  liquid state. These analyses will help determine the course ahead to a more complete understanding of the properties of this model.

#### ACKNOWLEDGMENTS

V.R.C. thanks the Centre for Development of Advanced Computing, Pune, India for computational resources through the project NumericalStudy-Magnets-PR and Sylvain Capponi for e-mail communication with helpful pointers regarding the usage of the GAP software package.

#### APPENDIX

As mentioned in the text, the implementation of the conservation of  $S_z^{\text{total}}$  and spin inversion symmetry for exact diagonalization is not sufficient to get a nondegenerate ground state in each symmetry sector. In order to analyze orthogonal eigenvectors with distinct symmetry labels, we use the

following permutation of site indices, which is an element of the automorphism group of the graph and results in a symmetry of the Hamiltonian, for any  $J_2$ :

$$(0,5,8,10)(1,3,9,7)(2,11,6,4)(12,13,15,14), \\ (16,22,24,18)(17,26,25,21)(19,20,23,27), \\ (28,30,31,29)(32,34,35,33).$$

Throughout the text, this site permutation is referred to as  $\mathcal{P}$ . Here,  $(a,b,c,d)$  denotes a cycle representing the site

permutation ( $a \rightarrow b \rightarrow c \rightarrow d \rightarrow a$ ). The above permutation is an element of order 4 of the automorphism group for the graph representing the considered lattice. The evaluated eigenvectors belong either to eigenvalues 1 or  $-1$  as indicated in the text. We note that this is one of several possible elements of the symmetry group of the Hamiltonian. It would be perfectly legitimate to choose another permutation, it would merely result in a different linear combination of the eigenvectors. Information regarding the automorphism group has been extracted using the GAP, GRAPE, and NAUTY software packages.

- 
- [1] G. H. Wannier, *Phys. Rev.* **79**, 357 (1950).  
 [2] P. W. Anderson, *Phys. Rev.* **102**, 1008 (1956).  
 [3] J. S. Gardner, M. J. P. Gingras, and J. E. Greedan, *Rev. Mod. Phys.* **82**, 53 (2010).  
 [4] K. Kimura, S. Nakatsuji, and T. Kimura, *Phys. Rev. B* **90**, 060414 (2014).  
 [5] L. Clark, G. J. Nilsen, E. Kermarrec, G. Ehlers, K. S. Knight, A. Harrison, J. P. Attfield, and B. D. Gaulin, *Phys. Rev. Lett.* **113**, 117201 (2014).  
 [6] Y. Iqbal, T. Müller, K. Riedl, J. Reuther, S. Rachel, R. Valentí, M. J. P. Gingras, R. Thomale, and H. O. Jeschke, *Phys. Rev. Mater.* **1**, 071201 (2017).  
 [7] A. B. Harris, A. J. Berlinsky, and C. Bruder, *J. Appl. Phys.* **69**, 5200 (1991).  
 [8] H. Tsunetsugu, *Phys. Rev. B* **65**, 024415 (2001).  
 [9] H. Tsunetsugu, *J. Phys. Soc. Jpn.* **70**, 640 (2001).  
 [10] M. Isoda and S. Mori, *J. Phys. Soc. Jpn.* **67**, 4022 (1998).  
 [11] H. Tsunetsugu, *Prog. Theor. Exp. Phys.* **2017**, 033101 (2017).  
 [12] E. Berg, E. Altman, and A. Auerbach, *Phys. Rev. Lett.* **90**, 147204 (2003).  
 [13] B. Canals and C. Lacroix, *Phys. Rev. Lett.* **80**, 2933 (1998).  
 [14] R. Moessner, S. L. Sondhi, and M. O. Goerbig, *Phys. Rev. B* **73**, 094430 (2006).  
 [15] O. Tchernyshyov, R. Moessner, and S. L. Sondhi, *Europhys. Lett.* **73**, 278 (2006).  
 [16] F. J. Burnell, S. Chakravarty, and S. L. Sondhi, *Phys. Rev. B* **79**, 144432 (2009).  
 [17] J. H. Kim and J. H. Han, *Phys. Rev. B* **78**, 180410 (2008).  
 [18] Y. Huang, K. Chen, Y. Deng, N. Prokof'ev, and B. Svistunov, *Phys. Rev. Lett.* **116**, 177203 (2016).  
 [19] J. Cullum and R. Willoughby, *Lanczos Algorithms for Large Symmetric Eigenvalue Computations* (Birkhäuser, Boston, 1985).  
 [20] X. G. Wen, F. Wilczek, and A. Zee, *Phys. Rev. B* **39**, 11413 (1989).  
 [21] C. Waldtmann, H.-U. Everts, B. Bernu, C. Lhuillier, P. Sindzingre, P. Lecheminant, and L. Pierre, *Eur. Phys. J. B* **2**, 501 (1998).  
 [22] S. E. Palmer and J. T. Chalker, *Phys. Rev. B* **64**, 094412 (2001).  
 [23] J.-B. Fouet, M. Mambrini, P. Sindzingre, and C. Lhuillier, *Phys. Rev. B* **67**, 054411 (2003).  
 [24] L. Amico, R. Fazio, A. Osterloh, and V. Vedral, *Rev. Mod. Phys.* **80**, 517 (2008).  
 [25] A. M. Läuchli, J. Sudan, and R. Moessner, [arXiv:1611.06990](https://arxiv.org/abs/1611.06990).